Multiobjective Finite Control Set Model Predictive Control Using Novel Delay Compensation Technique for PMSM

Yaofei Han, *Member, IEEE*, Chao Gong, *Student Member, IEEE*, Liming Yan, *Student Member, IEEE*, Huiqing Wen, *Senior Member, IEEE*, Yangang Wang, *Senior Member, IEEE*, and Ke Shen, *Member, IEEE*

***Abstract*—This article proposes a new finite control set model predictive control (FCS-MPC) strategy that simultaneously evaluates two targeting control objectives including speed and currents in a single cost function, achieving high-performance single-closed-loop control structure. Besides, aiming at the calculation delay problem of the model predictive control controllers, a novel calculation delay compensation method by predicting the current variation within the delay time is proposed. In this article, an improved machine model that is especially designed for the multiobjective FCS-MPC operation is illustrated at first. Then, a new cost function that can evaluate the tracking performance of speed and *d*-axis current and the steady-state performance of the *q*-axis current is developed. Compared with the conventional FCS-MPC approaches, extra speed controllers are not needed so that the proposed control topology becomes simpler. Then, in order to tune the weighting factors for the speed and currents in the cost function, an efficient handling strategy containing two implementation procedures, state variable normalization and balance of state sensitivity to voltage alteration, is developed. Finally, a brand-new computation delay estimation and compensation technique based on the dual sampling within a control period is proposed to reduce the current and torque ripples during the control process. Comparative simulation and experiments conducted on a three-phase 1.5-kW permanent magnet synchronous machine drive system are employed to verify the effectiveness of the proposed techniques.**

***Index Terms*—Delay compensation, model predictive control (MPC), multiobjective, permanent magnet synchronous machine (PMSM), weighting factors.**

Manuscript received June 30, 2019; revised September 24, 2019 and December 25, 2019; accepted March 3, 2020. Date of publication March 8, 2020; date of current version June 23, 2020. Recommended for publication by Associate Editor M. Ordonez. *(Corresponding author: Chao Gong.)*

Yaofei Han is with the School of Electronic Information and Electrical Engineering, Shanghai Jiao Tong University, Shanghai 200240, China (e-mail: hanyaofei@126.com).

Chao Gong is with the Department of Electronic Engineering, University of York, York YO10 5DD, U.K. (e-mail: 1452101806@qq.com).

Liming Yan is with the School of Automobile, Chang'an University, Xi'an 710064, China (e-mail: liming123@mail.nwpu.edu.cn).

Huiqing Wen is with the Department of Electrical and Electronic Engineering, Xi'an Jiaotong-Liverpool University, Suzhou 215123, China (e-mail: huiqing.wen@xjtlu.edu.cn).

Yangang Wang is with the R&D Centre of CRRC Dynex Semiconductor, Ltd., Lincoln LN6 3LF, U.K. (e-mail: yangang.wang@dynexsemi.com).

Ke Shen is with the Shaanxi Key Laboratory of Small and Special Electrical Machine and Drive Technology, School of Automation, Northwestern Polytechnical University, Xi'an 710129, China (e-mail: kshen@nwpu.edu.cn).

Color versions of one or more of the figures in this article are available online at http://ieeexplore.ieee.org.

Digital Object Identifier 10.1109/TPEL.2020.2979122

I. Introduction

NOWADAYS, permanent magnet synchronous machines (PMSMs) characterized by high power and torque density, and high efficiency and compact structure have been heavily adopted in electric vehicles, computer numerical control machines, and other servo drives [1]–[3]. Usually, good operation properties (e.g., high dynamic and steady-state characteristics and low current and torque ripple) are highly required in these applications, placing intensive demands upon high-performance control strategies [4], [5].

Due to the merits of quick response, excellent constraint handling capability, and optimum control principle, model predictive control (MPC), which was proposed in 1970s, has been developed significantly in the field of motor drive [6], [7]. For example, MPC-based controllers have been designed to achieve various functions in the machine control systems. In [8] and [9], MPC is incorporated into the direct torque control methods, predicting and regulating the electromagnetic torque and flux of the PMSMs. Kwak *et al.* [10] propose a model predictive power control method for a permanent magnet synchronous generator to enhance the steady-state performance of the system. In addition, model predictive speed controllers (MPSC) are incorporated into the machine control topologies to achieve high-performance speed control dynamics in [11]–[14]. Another popular application is model predictive current control (MPCC), in which the currents are set as the targeting control objectives (TCO) [15]–[18]. In comparison with MPSC, the current ripples of the MPCC become lower without markedly sacrificing the dynamic performance. The above-mentioned MPC algorithms can be classified into two generic groups [19]. One extends on the conventional proportional–integral (PI) based vector control by replacing the PI controllers with one or more MPC-based controllers but still retaining a modulator to generate pulsewidth modulation signals, such as in [15] and [16]. The other totally discards the modulator and directly uses the output of the cost function to determine the optimal converter switching states, as in [17] and [18]. Comparatively speaking, the latter scheme, known as finite control set MPC (FCS-MPC), is much easier to implement, benefiting from a voltage vector lookup table, which can be obtained offline. At present, in the light of the easiness for implementation, compared with the former modulation-based strategy, the FCS-MPC method has more competitive

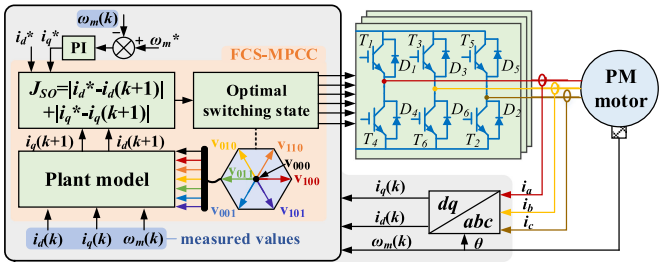

$i_{d,q}$: d, q-axis currents, $i_{d,q}^*$: reference d, q-axis currents, **v**: candidate voltages
ω_m: speed, ω_m^*: reference speed, θ: position, i_a, i_b, i_c: phase currents

Fig. 1. Structure of an FCS-MPCC-based drive system.

advantages so as to attract increasing attention in the PMSM drive applications [20]–[27].

Concerning the different TCOs included in the cost functions, there exist two types of commonly used FCS-MPC techniques: multiobjective FCS-MPC and single-objective FCS-MPC. The FCS model predictive torque control (FCS-MPTC), whose TCOs are the torque and flux, is the typical application of the multiobjective FCS-MPC theories [21], [22]. In the FCS-MPTC-based control systems, extra speed controllers (e.g., PI controller) are required for tracking the reference speed ω_m^* and generating the reference torque. When it comes to the single-objective FCS-MPC approaches, the MPCC-based controller in which the current is the only TCO is the most intensively studied topic [23], [24]. Similar to the FCS-MPTC method, the speed regulators cannot be eliminated either because they should be used for the q-axis reference current i_q^* generation, as shown in Fig. 1. Unluckily, the speed controllers contribute much to the complexity of the drive topology, and it is an uphill task to tune their parameters because of the lacking theoretical design procedures for the multitype-controller-based systems. In order to simplify the control topology, Preindl *et al.* [25]–[27] employ a new single-objective MPC method by only using one FCS-MPSC-based controller. This method only contains the speed control loop in the topology, resulting in that neither the steady state nor dynamic characteristics of the other machine states (e.g., current and torque) will be evaluated simultaneously. Besides, Formentini *et al.* [28]–[30] employ one single multiobjective FCS-MPC controller to control both currents and speed simultaneously. To improve the control performance of this kind of method, these studies focus on developing different disturbance and noise suppression techniques, leading to the fact that the cost function is relatively complex. It also needs to be mentioned that although this kind of method has been proven to be effective to improve the speed dynamics, many crucial challenges still require further discussion. For instance, scholars never stop looking for analytical weighting factor tuning methods and novel calculation delay handling strategies to enrich the correlative theories.

The main purpose of this article is to design an FCS-MPC-based controller that can meanwhile take multiple TCOs (speed and d- and q-axis currents) into account, achieving high-performance single-closed-loop control structure. Different from [28]–[30], the cost function of the new method is simplified without considering the external disturbances. However, the same to the traditional multiobjective FCS-MPC methods, the combination of the two variables in one single cost function is not a straightforward task because they are of different properties (units, magnitude in values, and state sensitivity to voltage change). Weighting factors must be introduced into the cost function for balancing the different control targets. Unfortunately, there are no ready-made standard analytical or numerical methods or control design theories to tune these parameters, and they are mainly determined based on the empirical procedures [31]. Consequently, the efficient weighting factor handling strategies should be especially developed for the novel model predictive speed and current controller.

Another typical problem of an FCS-MPC for PMSM drive systems is that the loads of calculations have to be executed during the switching state selection process, so the calculation time is long [32], [33]. The time delay between the state measurement and actuation would deteriorate the system performance if not considered, lessening the concept and effect of optimal control. Two-step prediction (TSP) strategy that uses the machine model shifted one step forward to calculate the manipulated voltages is explained in [34] and [35]. Although this scheme is simple to implement, it is not totally effective to accurately determine the optimum switching state because its implementation prerequisite is that the time delay equals to a control period.

This article proposes a multiobjective FCS-MPC strategy based on the novel calculation delay compensation method to achieve high-performance speed and current control. A hybrid cost function, which is based on the speed and current errors is developed to select the best voltage vector. In comparison with the traditional single-objective FCS-MPC, no extra speed controllers are employed anymore, simplifying the control topology greatly. Moreover, the reasons why the weighting factors have to be employed for the proposed MPC controller are explained explicitly, and an efficient handling strategy that contains two sequential implementation procedures is developed. Finally, the performance (especially steady-state performance) of the currents and output torque can be improved by using the proposed delay compensation method based on the dual sampling in one control period.

The structure of the rest article is as follows. Section II introduces the improved PMSM model that is suitable for designing the multiobjective FCS-MPC algorithms. In Section III, first, the structure of the proposed multiobjective FCS-MPC strategy is demonstrated. Then, the weighting factor solutions and the computation delay estimation and compensation procedures are detailed in this part. Section IV discusses the simulation and experimental results of the proposed algorithms. Finally, Section V concludes this article.

II. Improved Model for Multiobjective FCS-MPC

State-space model, which comprises no less than one differential equation, is capable of accurately reflecting the transient behaviors of a multivariable system, making itself well suited for PMSM MPC applications with further reference to the nonlinearization and strong coupling properties. The state-space

model that describes the electrical and mechanical dynamics of a PMSM in the direct-quadrature (dq) rotating frame is as follows, where the iron saturation and hysteresis loss are assumed negligible [19]:

$$\frac{di_d}{dt} = -\frac{R_s}{L_d}i_d + \frac{L_q}{L_d}p\omega_m i_q + \frac{u_d}{L_d} \tag{1}$$

$$\frac{di_q}{dt} = -\frac{L_d}{L_q}p\omega_m i_d - \frac{R_s}{L_q}i_q + \frac{u_q}{L_q} - \frac{\Psi_f}{L_q}p\omega_m \tag{2}$$

$$\frac{d\omega_m}{dt} = \frac{1}{J}(1.5p(\Psi_f i_q + (L_d - L_q)i_d i_q) - T_l) \tag{3}$$

where i_d and i_q are the stator dq-axis currents and u_d and u_q are the dq-axis control voltages. L_d and L_q are the dq-axis inductance, and $L_d = L_q$ for a surface-mounted PMSM. The stator winding resistance is R_s. T_l and ω_m are the load torque and rotor mechanical angular speed, respectively. Then, p represents the number of pole pairs and Ψ_f is the flux linkage. J is the overall inertia considering load.

In order to predict the future states, the continuous domain model must be discretized in a time step of T (control period). When the forward Euler discretization is applied to (1) and (2), the predicting plant model (PPM) can be expressed as

$$i_d(k+1) = \frac{L_d - TR_s}{L_d}i_d(k) + \frac{TL_q p}{L_d}\omega_m(k)i_q(k) + \frac{T}{L_d}u_d(k) \tag{4}$$

$$i_q(k+1) = -\frac{TL_d p}{L_q}\omega_m(k)i_d(k) + \frac{L_q - TR_s}{L_q}i_q(k) + \frac{T}{L_q}u_q(k) - \frac{T\Psi_f p}{L_q}\omega_m(k) \tag{5}$$

where $i_d(k)$, $i_q(k)$, and $\omega_m(k)$ are the states at the kth sampling instant. $i_d(k+1)$ and $i_q(k+1)$ are the predicting values at the $(k+1)$th period (t_{k+1}). The discretization operation cannot be applied to (3) because the speed alteration within the kth period is not directly determined by the manipulated variables $u_d(k)$ and $u_q(k)$ but it is a direct consequence of the overall currents in the cycle rather than just the initial currents at t_k. Considering this, take the definite integral of (3) between t_k and t_{k+1} and the PPM for speed estimation turns

$$\omega_m(k+1) = \frac{1.5p\Psi_f}{J}\int_{t_k}^{t_{k+1}} i_q dt + \frac{L_d - L_q}{J}\int_{t_k}^{t_{k+1}} i_d i_q dt - \frac{1}{J}\int_{t_k}^{t_{k+1}} T_l dt + \omega_m(k) \tag{6}$$

where $\omega_m(k+1)$ is the speed at t_{k+1}. Usually, the control period T is very short, so an appropriate equivalence that i_q and $i_d i_q$ experience linear changes under the control of $u_d(k)$ and $u_q(k)$, and the external load torque T_l remains constant at $T_l(k)$ over the period that can be made. In this case, (6) can be rewritten as

$$\omega_m(k+1) = \frac{3p\Psi_f T}{4J}(i_q(k+1) - i_q(k)) - \frac{T_l(k)T}{J} + \omega_m(k) + \frac{(L_d - L_q)T}{2J}(i_d i_q(k+1) - i_d i_q(k)). \tag{7}$$

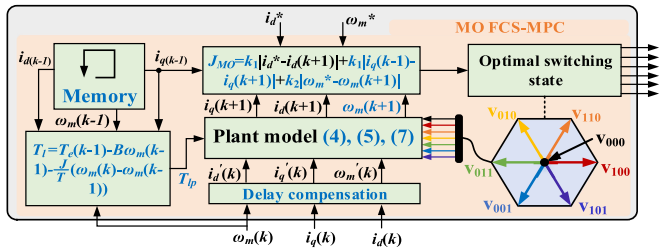

Fig. 2. Structure of multiobjective FCS-MPC-based controller.

Obviously, when predicting the speed state, the future currents should be calculated by (4) and (5) in advance. It should be addressed that only by doing this can $\omega_m(k+1)$ be associated with the manipulated voltages.

As for the candidate control voltages, in practice, a total of seven phase voltage vectors ($\mathbf{v}_{000}$, $\mathbf{v}_{100}$, $\mathbf{v}_{110}$, $\mathbf{v}_{010}$, $\mathbf{v}_{011}$, $\mathbf{v}_{001}$, and $\mathbf{v}_{101}$) are among the alternatives for a two-level inverter

$$\mathbf{v}_{s_a s_b s_c} = \begin{bmatrix} v_a \\ v_b \\ v_c \end{bmatrix} = \frac{V_{\mathrm{dc}}}{3}\begin{bmatrix} 2 & -1 & -1 \\ -1 & 2 & -1 \\ -1 & -1 & 2 \end{bmatrix}\begin{bmatrix} s_a \\ s_b \\ s_c \end{bmatrix} \tag{8}$$

where $[s_a, s_b, s_c]^T$ consisting of $[0, 0, 0]^T$, $[1, 0, 0]^T$, $[1, 1, 0]^T$, $[0, 1, 0]^T$, $[0, 1, 1]^T$, $[0, 0, 1]^T$, and $[1, 0, 1]^T$ are the switching states. V_{dc} is the dc-link voltage. $[v_a, v_b, v_c]^T$ are the terminal phase voltages. By means of *abc*/*dq* transformation, the control voltage sets to be substituted into PPM for prediction can be expressed as

$$\begin{bmatrix} u_d(k) \\ u_q(k) \end{bmatrix} = \frac{2}{3}\begin{bmatrix} \cos\theta & \frac{\sqrt{3}\sin\theta - \cos\theta}{2} & \frac{-\sqrt{3}\sin\theta - \cos\theta}{2} \\ -\sin\theta & \frac{\sin\theta + \sqrt{3}\cos\theta}{2} & \frac{\sin\theta - \sqrt{3}\cos\theta}{2} \end{bmatrix} \cdot \mathbf{v}_{s_a s_b s_c}. \tag{9}$$

III. Multiobjective FCS-MPC Algorithm

The implementation procedures of an FCS-MPC algorithm can be summarized as follows: the measured currents and speed as well as the seven manipulated voltages are substituted into the PPM to predict the next step's states, and then the predicted values are evaluated by a cost function so as to select the optimal control voltage to be applied. In this process, the cost function serves as the key component for optimizing calculation, and it determines whether an FCS-MPC-based controller is a so-called single-objective or multiobjective scheme. In order to clearly compare the differences between a single-objective controller and the proposed approach, the cost function of an FCS-MPCC-based controller (see Fig. 1), which only regards the current as the control target, is demonstrated

$$J_{SO} = (i_d^* - i_d(k+1))^2 + (i_q^* - i_q(k+1))^2 \tag{10}$$

where i_d^* is the d-axis reference current and it can be set to zero if the flux-weakening operation is not required, and i_q^* is the q-axis reference current.

A. Structure of a Multiobjective FCS-MPC Method

Fig. 2 depicts the structure of a dual-objective (speed and current) FSC-MPC strategy. In comparison with the single-objective FCS-MPCC method, the explanations of the new algorithm are detailed as follows.

Most crucially, the speed and current performance are assessed by a novel multiobjective cost function

$$J_{MO} = k_1(i_d^* - i_d(k+1))^2 + k_1(i_q(k-1) - i_q(k+1))^2 + k_2(\omega_m^* - \omega_m(k+1))^2. \quad (11)$$

It can be noted that the proposed algorithm aims to track the d-axis current and speed references (i_d^* and ω_m^*), but an extra term of absolute error between the previous q-axis current $i_q(k-1)$ and $i_q(k+1)$ is also incorporated into the cost function. The reason for this configuration includes that it is impossible to simultaneously and precisely compel the rotating speed and q-axis current to track the manually set references in a PMSM by one sole MPC-based controller and, hence, $(i_q^* - i_q(k+1))^2$ cannot be integrated into the cost function. But from the other point of view, when the machine reaches the equilibrium state in the control process, the q-axis current ripples are expected to be further reduced so as to improve the steady-state performance of the PMSM. Practically, this performance characteristic can be evaluated by the current variations in the adjacent intervals. For the purpose of lowering the fluctuations of the q-axis current, which is directly related to the output electromagnetic torque, we import $(i_q(k-1) - i_q(k+1))^2$ into the multiobjective cost function. It should be mentioned that because the cost function is able to evaluate both the current and speed characteristics it is unnecessary to track a q-axis reference, so the speed controller is eliminated in the multiobjective FCS-MPC control structure.

Second, a load torque observer is integrated into the proposed controller. In (7), the real-time load torque should be used for predicting the future speed information. But a physical load torque sensor is usually not installed in the PMSM for the sake of cost reduction. In this case, a new issue that how to determine $T_l(k)$ arises. Guzinski *et al.* [36] present a theoretical solution to the problem by designing an observer to estimate T_l, but it does not explain the explicit discretization procedures. In this article, considering that the sampling period T is short (typically 0.2 ms), we make an appropriate assumption that the contemporary load torque is equal to that in the $(k-1)$th cycle. Then, a discrete torque estimator can be deduced by applying the backward Euler technique to the mechanical dynamic equation, that is

$$T_{lp}(k) = T_e(k-1) - B\omega_m(k-1) - \frac{J}{T}(\omega_m(k) - \omega_m(k-1)) \quad (12)$$

where T_{lp} is the observed load torque, and T_e is the output electromagnetic torque of the machine

$$T_e(k-1) = 1.5p(\Psi_f i_q(k-1) + (L_d - L_q) i_d(k-1) i_q(k-1)). \quad (13)$$

Third, the time delay caused by substituting the seven alternative voltages one by one into the plant model to calculate the future states is compensated, which will be beneficial to the system performance. The detailed compensation strategy is explained in Section III-C.

So far, the system control structure becomes simple by using a single multiobjective FCS-MPC-based controller to simultaneously control speed and currents. However, the weighting factors k_1 and k_2 must be adopted to balance the differences between the two kinds of control targets. To solve this problem, Section III-B proposes a brand-new handling method based on the state variable normalization (SVN) and the balance of state sensitivity to voltage alteration.

B. Weighting Factor Handling Strategy

One important reason why the weighting factors k_1 and k_2 are essential for the proposed multiobjective FCS-MPC-based controller is that the nature (unit and magnitude in value) of the speed and the d- and q-axis currents is different. Besides, the magnitude of the speed and current variations corresponding to the same voltage alteration is different. In other words, the sensitivity of the current and speed (response variables) to the voltage variations (control variables) is different. Unlike an FCS-MPTC method of which TCOs (torque and flux) are totally independent, resulting in that the importance of the two TCOs to switching state selection varies, the TCOs (speed and currents) of the proposed strategy are corelated. Specifically, the speed alteration is the consequence of current variation, as is illustrated by the machine model (3). Therefore, the importance of the speed and currents in the cost function should be the same without considering their sensitivity to voltage variations. Aiming at these two aspects, the weighting factor tuning strategy for the proposed multiobjective FCS-MPC-based controller can be achieved by following two sequential steps: SVN, and balance of state sensitivity to voltage alteration.

1) State Variable Normalization: The definition of SVN can be described as follows: the state variables, including current, speed, and voltage, are expressed as the fractions of the defined base quantities. After SVN, the large imparity in the magnitude and units of different variables can be removed. Namely, the representations of all variables in the system become uniform with per unit values (the unit is p.u. and the magnitude of values ranges from -1 to 1). In this article, the base quantities for PMSM system normalization are especially designed as follows. First, the base voltage V_0 is defined as the maximum line-to-line voltage

$$V_0 = V_{\rm dc}. \quad (14)$$

Then, according to this normalization principle, the base current I_0 is

$$I_0 = \frac{2P_{\rm rated}}{\sqrt{3}V_{\rm dc}} \quad (15)$$

where $P_{\rm rated}$ is the rated power of the motor. The base speed ω_{m0} equals the value of rotor angular velocity (in rad/s) at which the machine develops 1 p.u. voltage at its terminals with zero current. According to the relationship (see [19]) between the

back electromotive force (EMF) and the rotor speed, the base speed can be derived as

$$\omega_{m0} = \frac{V_{\rm dc}}{\sqrt{3}k_0 C'_e \Psi_f} \tag{16}$$

where C'_e is the voltage constant, and k_0 is an adjusting constant.

After applying SVN to the drive system, the normalized state variables are

$$i_{dn} = \frac{i_d}{I_0},\ i_{qn} = \frac{i_q}{I_0},\ u_{dn} = \frac{u_d}{V_0},\ u_{qn} = \frac{u_q}{V_0},\ \omega_{mn} = \frac{\omega_m}{\omega_{m0}}. \tag{17}$$

Then the electrical and mechanical PPMs can be expressed as

$$\mathbf{x}_{en}(k+1) = \mathbf{A}_e \mathbf{x}_{en}(k) + \mathbf{B}_e \mathbf{u}_n(k) + \mathbf{d}_{en}(k) \tag{18}$$

$$\mathbf{x}_{mn}(k+1) = \mathbf{A}_m \mathbf{x}_{mn}(k) + \mathbf{A}_{ms}(\mathbf{x}_{en}(k+1) - \mathbf{x}_{en}(k)) + \mathbf{d}_{mn}(k) \tag{19}$$

where $\mathbf{A}_e = \begin{bmatrix} \frac{L_d - TR_s}{L_d} & 0 \\ 0 & \frac{L_q - TR_s}{L_q} \end{bmatrix}$, $\mathbf{B}_e = \begin{bmatrix} \frac{T}{L_d} & 0 \\ 0 & \frac{T}{L_q} \end{bmatrix}$, $\mathbf{A}_m = \begin{bmatrix} 0 & 0 \\ 0 & 1 \end{bmatrix}$ and $\mathbf{A}_{ms} = \begin{bmatrix} 0 & 0 \\ 0 & \frac{3p\Psi_f T}{4J} \end{bmatrix}$. $\mathbf{x}_e = [i_{dn}, i_{qn}]^T$, $\mathbf{u}_{en} = [u_{dn}, u_{qn}]^T$, $\mathbf{x}_{mn} = [0, \omega_{mn}]^T$, and $\mathbf{d}_{en}$ and $\mathbf{d}_{mn}$ are considered as the disturbances, which can be written as

$$\mathbf{d}_{en} = \left[\frac{TL_q p}{L_d} \omega_{mn} i_{qn}, -\frac{TL_d p}{L_q} \omega_{mn} i_{dn} - \frac{T\Psi_f p}{L_q} \omega_m \right]^T \tag{20}$$

$$\mathbf{d}_{mn} = \left[0, \frac{(L_d - L_q)T}{2J} (i_d i_q(k+1) - i_d i_q(k)) \right]^T. \tag{21}$$

2) Balance of State Sensitivity to Voltage Alteration: For the sake of simplicity, assume that $L_d = L_q = L_s$ and ignore the effects of mutual inductance. The machine models (5) and (7) can be expressed as

$$i_q(k+1) = \frac{L_s - TR_s}{L_s} i_q(k) - \frac{T\Psi_f p}{L_s} \omega_m(k) + \frac{T}{L_s} u_q(k) \tag{22}$$

$$\omega_m(k+1) = \frac{3p\Psi_f T}{4J} (i_q(k+1) - i_q(k)) - \frac{T_l T}{J} + \omega_m(k). \tag{23}$$

In addition to $u_q(k)$, a voltage disturbance $\triangle u_q(k)$ is assumed to be applied to the machine at t_k. It can be deduced that the current alteration $\triangle i_q(k+1)$ caused by $\triangle u_q(k)$ in one cycle can be described as

$$\Delta i_q(k+1) = \frac{T}{L_s} \Delta u_q(k) \tag{24}$$

while the speed alteration $\triangle \omega_m(k+1)$ caused by $\triangle u_q(k)$ is

$$\Delta \omega_m(k+1) = \frac{3p\Psi_f T}{4J} \Delta i_q(k+1). \tag{25}$$

Obviously, the currents in the machine are more sensitive to the voltage changes. In order to balance the state sensitivity to voltage variation differences between the two variables, the weighting factors can be set as

$$k_1 = 1, \quad k_2 = \frac{4J}{3p\Psi_f T}. \tag{26}$$

Then, the magnitude of the speed and current variations caused by the same voltage change within one control period will stand at the same level. Note that the weighting factor k_2 is related to the sampling period T, representing that the discretization scheme is an important factor that influences the optimization operation of the multiobjective FCS-MPC-based controller.

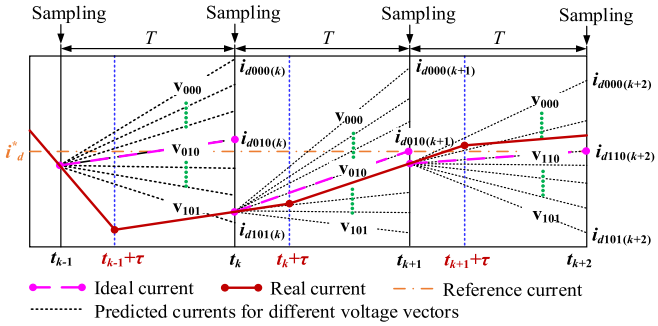

Fig. 3. Comparison between the ideal condition and the real condition.

C. Novel Computation Delay Compensation Strategy for Ripple Reduction

The goal of the cost function is to suppress the current and speed tracking errors to the most degree, but it will be blocked by the calculation delay. For the sake of convenience, this part takes i_d as an example to analyze the issue, and a comparison between the ideal condition and the real condition is shown in Fig. 3. It can be seen that between t_{k-1} and t_k, $\mathbf{v}_{010}$ is evaluated as the best voltage vector with the measured information available at the beginning of this period. However, the actuation action is not applied at t_{k-1} but at $t_{k-1} + \tau$, where τ is the computation delay, leading to that the current locus cannot be controlled as expected and some deviation occurs after a control period. In this case, $\mathbf{v}_{010}$ may not be the best solution, and this phenomenon cannot be self-healed in the later cycles, such as the $(k+1)$th and $(k+2)$th period.

The traditional TSP strategy is proposed with an assumption of that $\tau = T$ and the concrete compensation procedures can be referred to in [35]. But, in practice, the delay time cannot exceed a control period, as shown in Fig. 3. In view of the problem, this article presents a compensation scheme on the basis of dual sampling and delay time estimation [see Fig. 4(a)]. Another remarkable feature can be noticed in Fig. 4(b) that instead of operating on the predicted states, the new method will calibrate the measured values before predicting the future states.

1) τ Estimation: In order to estimate and compensate the delay time, assume that the real current will shift linearly in accordance with the predicted trend and the computation delay remains constant in each control period.

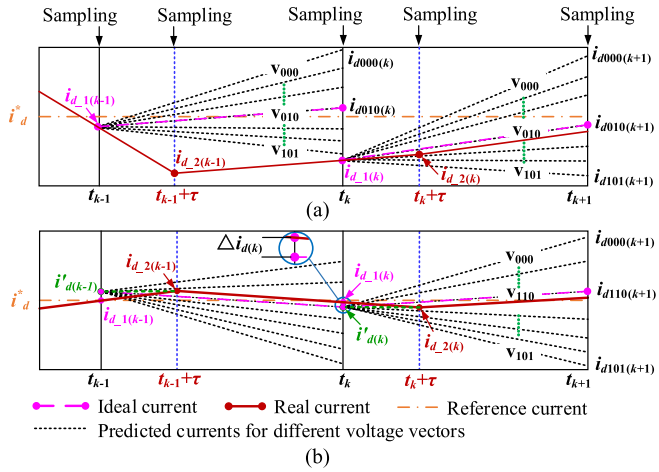

Fig. 4. Proposed compensation method. (a) Delay time calculation. (b) Compensation.

When estimating τ, the proposed multiobjective FCS-MPC algorithm without compensation will be applied. But an obvious feature can be witnessed that there are two sampling points in each control period, one of which is at the start of a period. The other is at the end of voltage selection, where the computation work is finished. In Fig. 4(a), the sampling currents over $t_{k-1}, \ldots, t_k$ and $t_k, \ldots, t_{k+1}$ are $i_{d\_1(k-1)}$, $i_{d\_2(k-1)}$ and $i_{d\_1(k)}$, $i_{d\_2(k)}$, respectively. The delay can be calculated by

$$\tau = \frac{|i_{d\_2(k)} - i_{d\_1(k)}|}{|i_{d\_2(k)} - i_{d\_2(k-1)}|} \cdot T. \tag{27}$$

2) Compensation: Since τ is obtained, the detailed compensation procedures are as follows at t_k.

1) First measurement and *abc*/*dq* transformation: Use sensors to detect the real phase currents, rotor position, and speed and transform the measured phase currents to the *dq*-axis currents.
2) Compensation: Predict the current variation $\triangle i_{d(k)}$ in τ [see Fig. 4(b)]

$$\Delta i_{d(k)} = \frac{i_{d\_1(k)} - i_{d\_2(k-1)}}{T - \tau} \cdot \tau \tag{28}$$

where $i_{d\_2(k-1)}$ is also the sampling current in the last interval, and the current used for prediction is

$$i'_{d(k)} = i_{d\_1(k)} + \Delta i_{d(k)}. \tag{29}$$

Following the above approach, the compensated q-axis current $i'_q(k)$ and speed $\omega'_m(k)$ can also be calculated. Then, the control process is as the following.

3) Prediction: Use $i'_d(k), i'_q(k), \omega'_m(k)$, and T_l to estimate the future states for all the seven candidate voltage vectors.
4) Evaluation: Substitute all the predicted values into the cost function and determine the optimal voltage vector.
5) Second measurement: Repeat step 1) to get currents $(i_{d\_2}(k), i_{q\_2}(k))$, position, and speed $\omega_{m\_2}(k)$.
6) Switching state application: Apply the corresponding optimum switching state to the drive.

TABLE I
MOTOR AND CONTROL PARAMETERS

Parameter	VALUE	Unit
stator winding resistance R_s	0.6383	Ω
d-axis inductance L_d	2	mH
q-axis inductance L_q	2	mH
the number of pole pairs p	4	-
moment of inertia J	0.13	kg·m^2
voltage constant C'_e	5.01	-
permanent magnet flux linkage Ψ_f	0.085	Wb
DC-link voltage V_{DC}	310	V
sampling time T	0.0001	s
safety current I_{safe}	60	A
rated torque T_{rated}	5	Nm
rated power P_{rated}	1.5	kW

Theoretically, the real current at $t_k + \tau$ will reach the previously predicted value, which means that the proposed multiobjective FCS-MPC method obeys the optimum control rule just with a delay of τ.

IV. VERIFICATIONS

The performance of the proposed multiobjective FCS-MPC without and with delay compensation is tested and compared by the means of simulation and experiments. The motor and control parameters of the PMSM prototype are consistent with Table I.

A. Simulation Results

For the sake of comprehensive discussion, the following verifications are included in this article. First, in order to comparatively explain the control performance, apart from the proposed multiobjective FCS-MPC method, the traditional double closed-loop FCS-MPCC strategy [see Fig. 1] is tested as well. Second, to validate the effectiveness of the proposed calculation delay technique, the performance characteristics of the proposed method without and with compensation are compared. Third, to verify that the proposed calculation delay strategy is superior to the traditional TSP technology, the steady-state current performance of the proposed FCS-MPC method compensated by the two methods is analyzed.

The verification procedures for the traditional and proposed methods without delay compensation are as follows. The machine speeds up from standstill to 100 rad/s at first, after which it will stabilize until 1.0 s when a constant load of 5 N·m is suddenly applied. From 1.5 s, the reference speed is set as 200 rad/s, while the motor begins to slow down from 2.5 s. After removing the external load at 3.0 s, the rotating speed of the machine continues to decline until it reaches zero.

1) Analysis on the State-State Performance: Figs. 5 and 6 illustrate the control performance of the traditional and proposed multiobjective FCS-MPC algorithms without delay compensation. For the two methods, it can be noted that the motor speed remains stable after it arrives at the setpoint no matter whether the machine is loaded or not during the whole test range. Besides, the average value of the d-axis current can level off at zero. These indicate that the proposed multiobjective FCS-MPC has marked speed and current tracking capability without steady-state errors.

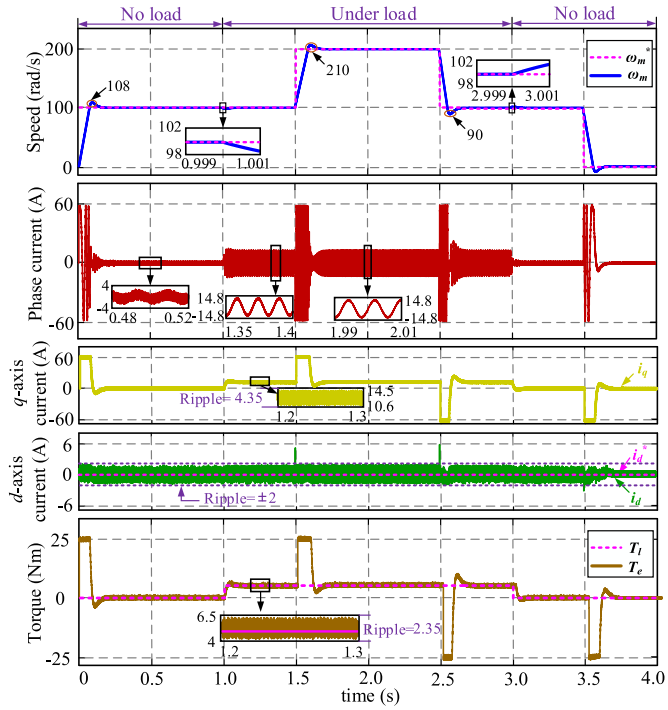

Fig. 5. Performance of the traditional double closed-loop FCS-MPCC algorithm without delay compensation.

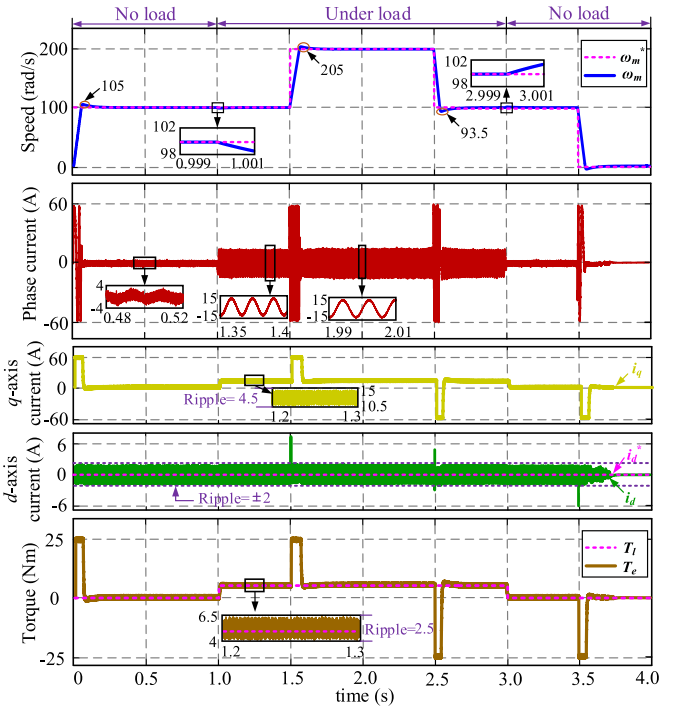

Fig. 6. Performance of the proposed multiobjective FCS-MPC algorithm without delay compensation.

However, visible current and torque ripples can be witnessed in both Figs. 5 and 6. Specifically, under load conditions, the peak-to-peak ripple of the q-axis for the traditional method is 4.35 A, equaling nearly 33.8% of the average value (12.55 A), and the d-axis current and torque ripples are about 4 A and 2.35 N·m, respectively. Comparatively speaking, the d- and q-axis current and the torque ripples of the proposed multiobjective method are 4 A, 4.5 A (37.5% of the average value), and 2.5 N·m, respectively. As for the no-load cases, the magnitude of the current and torque ripples stands at very similar position with rated load conditions for both of the methods. It can be noted that the proposed multiobjective FCS-MPC controller has as good steady-state performance as the traditional double closed-loop FCS-MPCC method, indicating that the proposed multiobjective FCS-MPC-based controller is totally qualified for regulating speed as well as current without using a speed controller to generate the q-axis reference current.

2) Analysis on the Dynamic Performance: Dynamic performance evaluation of the control system needs to consider the following aspects, namely, settling time, speed and current overshoot, and robustness to abrupt load variation.

During acceleration, first, the rise time of the traditional FCS-MPCC method is nearly 0.15 s, while it is about 0.1 s for the proposed MPC algorithm regardless of load or no-load conditions. Second, between 0 and 0.5 s, the speed overshoot in Figs. 5 and 6 is 8 rad/s (8%) and 5 rad/s (5%), respectively, and between 1.5 and 2 s, it is 10 rad/s and 5 rad/s, respectively. These represent that the proposed method has slightly better dynamics than the traditional one, complying with the results in [28]. Moreover, because the output of the speed controller (q-axis reference) of the traditional method is constrained as 60 A and we use the current constraint method, which is detailed in [19], both the phase and q-axis currents just jump to the safety level during acceleration for both of the methods. When the q-axis current reaches 60 A, the maximum output electromagnetic torque is about 25 N·m. Moreover, the d-axis current fluctuates clearly at 1.5 s, which is caused by cross-coupling effect. In terms of deceleration, the settling time and speed overshoot are about 0.15 s and 10 rad/s (10%) at 2.5 s for the traditional method and for the multiobjective strategy, they are 0.1 s and 6.5 rad/s (6.5%), respectively. In this process, the largest phase and the q-axis current are both nearly -60 A, which stands at the opposite position with acceleration. Similarly, the d-axis current witnesses some fluctuations at 2.5 and 3.5 s. When the load is imposed and removed from the motor, only a speed deviation of 2 rad/s appears for both the traditional method and the proposed strategy, and their output electromagnetic torques can quickly reach the expected level. These illustrate that the proposed multiobjective FCS-MPC algorithm has as strong robustness to torque variations as the double closed-loop structure. Overall, from the perspective of dynamics, the proposed multiobjective method is qualified for high-performance control.

Fig. 7 demonstrates the simulation results of the proposed FCS-MPC algorithm with delay compensation. As to the experimental setup, the algorithm is implemented to calculate the delay τ before 0.25 s, after which the proposed algorithm launches. Compared with Fig. 6, the advantage of the improved method is mainly reflected by the steady-state performance (the dynamic performance is similar), especially the current and torque ripples. In detail, before 0.25 s, the ripples of the q-axis

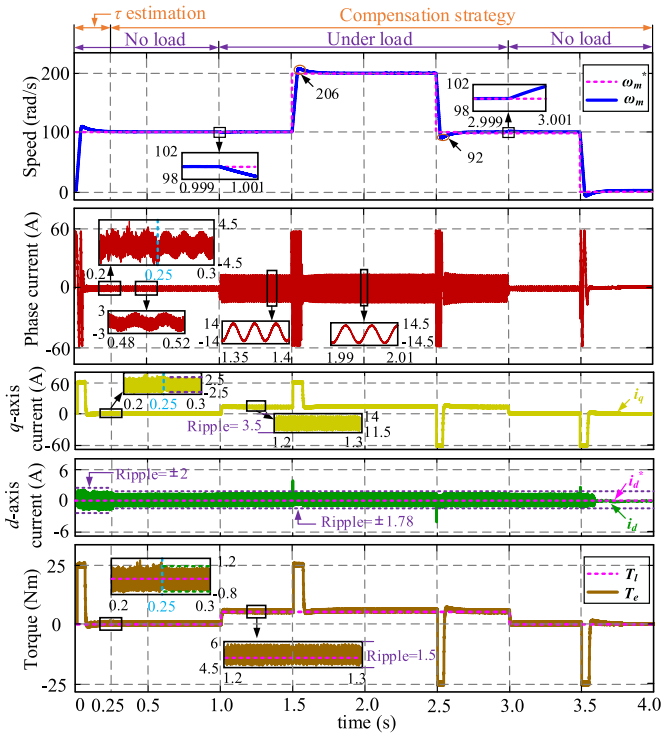

Fig. 7. Performance of the proposed multiobjective FCS-MPC algorithm with delay compensation.

TABLE II
PHASE CURRENT THD UNDER LOAD CONDITION

Method Type	Working States (rad/s)	THD (%)
Double loop FCS-MPCC without compensation	100	3.52
	200	5.83
Multi-objective FCS-MPC without compensation	100	3.85
	200	5.93
Multi-objective FCS-MPC with compensation	100	2.26
	200	4.35

current, d-axis current, and output torque ripples are 6 A, 4 A, and 2 N·m, respectively. However, they become nearly 5 A, 3.56 A, and 1.75 N·m with a drop of 16.7%, 11%, and 12.5% after compensation. The phase current ripple also experiences a visible declination before and after 0.25 s. Overall, the compensation method is conducive to high-performance control drive.

In order to more intuitively observe the control performance of the proposed method, Table II lists the total harmonic distortion (THD) simulation results for the phase currents under the rated load condition. At the speed of 100 rad/s, the phase current THD for the traditional double closed-loop FCS-MPCC method without compensation, proposed multiobjective FCS-MPC method without compensation and proposed method with compensation is 3.53%, 3.85%, and 2.26%, respectively, and at the speed of 200 rad/s, they are 5.83%, 5.93%, and 4.35%, respectively. In the first place, the performance of the proposed FCS-MPC method is very similar to the traditional strategy, further proving that the proposed method is of high performance. Second, after delay compensation, the current performance is greatly improved, indicating that the calculation delay is a key factor that influences

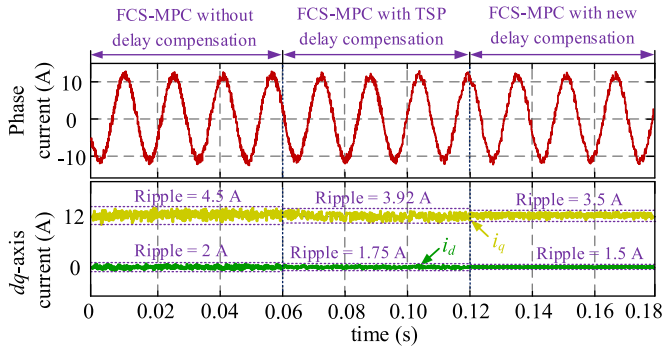

Fig. 8. Current performance under the control of proposed multiobjective FCS-MPC with different delay compensation methods.

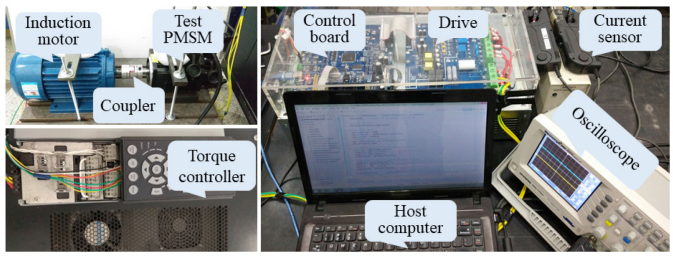

Fig. 9. Experimental test equipment including PMSM, load, oscilloscope, and controller.

the steady-state performance. Finally, it is interesting to see that the THD at the rated operation point is larger than that at the low-speed cases. Many reasons have caused this phenomenon, one of which is the dead time effect.

To compare the performance of the traditional TSP delay compensation method and the novel one, the following verification setup is designed. The machine rotates at the speed of 100 rad/s with rated load. The proposed multiobjective FCS-MPC algorithm without delay compensation is used before 0.06 s, in which the time delay is computed. Between 0.06 and 0.12 s, the algorithm with TSP compensation (see [34]) is adopted, and afterward, the proposed algorithm is employed to control the motor. Fig. 8 illustrates the current performance in the whole control process. It can be seen that both of the compensation methods are effective to suppress the current ripples so as to improve the steady-state performance. But it deserves to be mentioned that the new compensation method is superior to the traditional one because it obeys the optimal control principle. Specifically, the d- and q-axis current ripples are 1.75 and 3.92 A for the TSP compensation strategy, while they are 1.5 and 3.5 A, respectively, for the new technique. In term of the phase current THD, it is 2.85% for the conventional compensation method, which is slightly larger than that (see Table II) for the novel dual-sampling-based strategy.

B. Experimental Results

The experimental equipment is shown in Fig. 9. The system parameters are consistent with Table I as well. A common dc power supply is available at 310 V. Insulated gate bipolar

TABLE III
TIME DELAY IN 15 DIFFERENT PERIODS

*k*th period	Delay (ms)	*k*th period	Delay (ms)	*k*th period	Delay (ms)
1	0.024	6	0.026	11	0.026
2	0.025	7	0.025	12	0.024
3	0.026	8	0.024	13	0.025
4	0.025	9	0.024	14	0.025
5	0.027	10	0.023	15	0.024

transistor modules, FP25R12KT3, constitute the voltage inverter with the control frequency of 10 kHz. The proposed algorithms are implemented on a DSP TMS320F28335 control board. Then, it is unnecessary to provide the expansion of VC and SMO. The real rotor position is detected by a 2500-line rotary encoder in this article. M (frequency-measuring method) and T (period-measuring method) methods are used for measuring the relatively high and the low rotating speed, respectively [37]. It deserves to be mentioned that according to (11), the updating frequency for speed equals that for currents (namely, the control frequency 10 kHz), so the test speed range that can optimally show the performance of the proposed method should be over 60 r/min in this article. Hall current sensors, HIOKI 3275 Clamp on Probe, are used to measure the phase currents, while the motor *d*- and *q*-axis currents are calculated and recorded by the digital controller. An induction motor driven by an Automation Drive FC 301 with torque control mode, is coupled to the test machine, providing the required load torque.

Apart from comparing the performance of the traditional FCS-MPCC method and the proposed multiobjective FCS-MPC method, the experiment will also be carried out to compare the control performance before and after delay compensation. For the sake of analytical simplicity, the delay time will be tested using the proposed delay estimation strategy beforehand in this part. Under no-load condition, the delay time is measured when the machine is controlled by the multiobjective FCS-MPC algorithm. Table III records the delay value in fifteen different control periods. It should be noted that the average delay of the test drive system is about 0.0258 ms, accounting for 25.8% of one single cycle. Undoubtedly, this will influence the control performance.

By contrast to the simulation procedures, the experimental setup without considering online delay estimation is as follows. The machine speed is set as 100 rad/s under no-load condition at first, after which it will maintain constant until 4.0 s when the rated load of 5 N·m is applied. From 6.0 s, the machine speed rises to 200 rad/s, while the motor decelerates at 10.0 s. At 12.0 s, the load is removed, and then the reference speed is set as 10 rad/s (ultra-low speed) at 14 s. Figs. 10–12 show the experimental results of the traditional FCS-MPCC method, the proposed multiobjective FCS-MPC method without delay compensation, and the proposed FCS-MPC approach with delay compensation, respectively.

On the one hand, similar to the simulation results, Figs. 10 and 11 illustrate that the proposed method has as good steady-state performance as the FCS-MPCC method regardless of the machine speed and load conditions. First, the machine speed

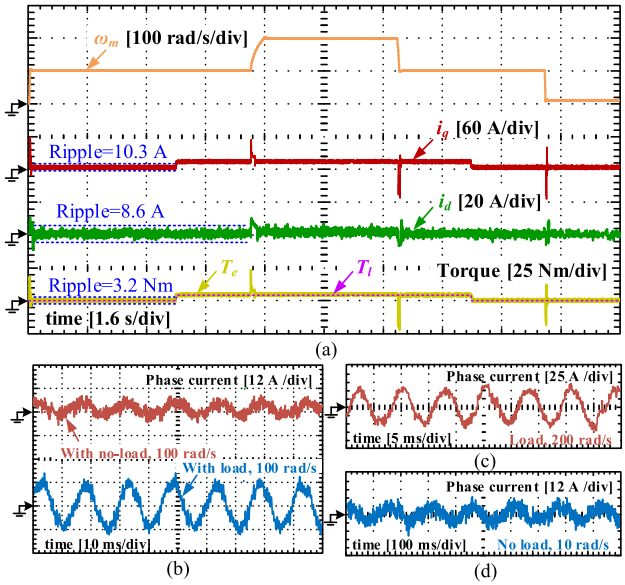

Fig. 10. Experimental performance of the traditional double closed-loop FCS-MPCC algorithm without delay compensation. (a) Speed, *d*-axis current, *q*-axis current, and torque. (b) Phase currents under no-load and load conditions at 100 rad/s. (c) Phase current under load condition at 200 rad/s. (d) Phase current under no-load condition at 10 rad/s.

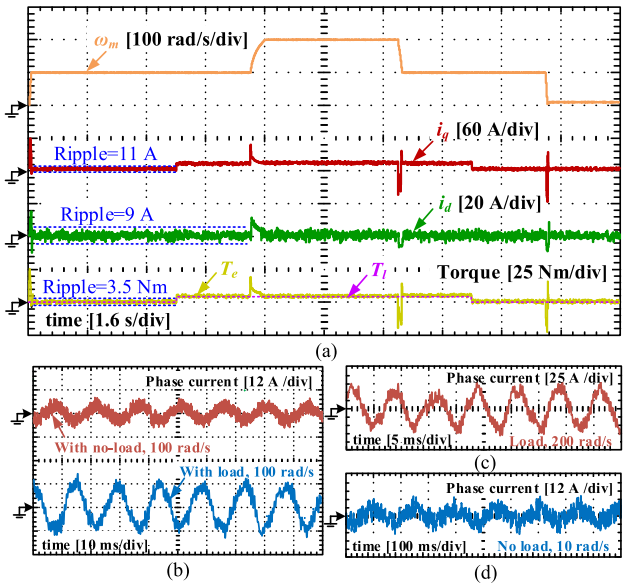

Fig. 11. Experimental performance of the proposed multiobjective FCS-MPC algorithm without delay compensation. (a) Speed, *d*-axis current, *q*-axis current, and torque. (b) Phase currents under no-load and load conditions at 100 rad/s. (c) Phase current under load condition at 200 rad/s. (d) Phase current under no-load condition at 10 rad/s.

can track the targeted values only with small fluctuations (less than 2 rad/s) in the stable states and the average value of the *d*-axis current is zero ($i_d^* = 0$). No static errors are seen, so the speed and current tracking properties for the two methods are good. Second, in terms of the *q*-axis current, they are both slightly higher than zero under the no-load conditions, which is caused by the friction, they level off at nearly 12 A with small fluctuations under load cases. Third, the output electromagnetic

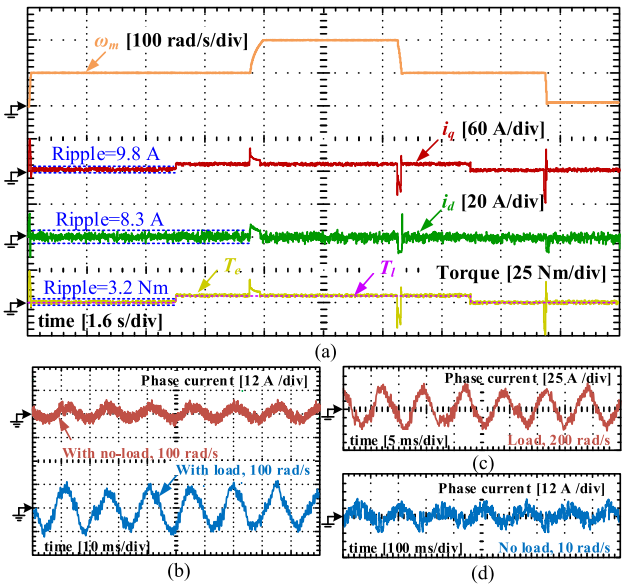

Fig. 12. Experimental performance of the proposed multiobjective FCS-MPC algorithm with delay compensation. (a) Speed, *d*-axis current, *q*-axis current, and torque. (b) Phase currents under no-load and load conditions at 100 rad/s. (c) Phase current under load condition at 200 rad/s. (d) Phase current under no-load condition at 10 rad/s.

TABLE IV
PHASE CURRENT THD UNDER LOAD CONDITION

Method Type	Working States (rad/s)	THD (%)
Double loop FCS-MPCC without compensation	100	8.52
	200	11.26
Multi-objective FCS-MPC without compensation	100	9.45
	200	12.1
Multi-objective FCS-MPC with compensation	100	7.96
	200	10.63

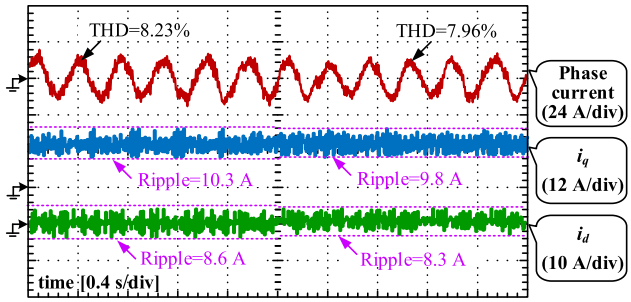

Fig. 13. Current performance under the control of proposed multiobjective FCS-MPC with different delay compensation methods.

torque of the machine in Figs. 10 and 11 is consistent with the external load, indicating that the PMSM drive system can work normally under the rated load conditions. Finally, when it comes to the variable ripples, the *d*- and *q*-axis current and the torque ripples of the proposed method are 9 A, 11 A, and 3.5 N·m, and for the FCS-MPCC strategy, they are 8.6 A, 10.3 A, and 3.2 N·m, respectively. In accordance with the simulation results, the steady-state performance differences between the two methods are small. On the other hand, interestingly, the settling time of the traditional FCS-MPCC method and the proposed strategy is very similar for the test bench. Over the low-speed range (0–100 rad/s), it is about 0.1 s, while it is nearly 0.3 s over the higher speed range (100–200 rad/s). This happens because a relatively smaller *q*-axis current has been generated during acceleration from 100 to 200 rad/s in the experiment. But the deceleration characteristics show a pretty similar trend to the simulation results. Moreover, due to the extra speed controller used in the topology of FCS-MPCC method, the speed experiences small overshoot regardless of acceleration and deceleration in Fig. 10, but it is modest in Fig. 11. In terms of the system robustness against load disturbances, the machine speed can remain stable even if the load is suddenly imposed or removed for the new method, which is the same to the double loop approach. Finally, when the *q*-axis current reaches ± 60 A in the transient process, the output electromagnetic torque in Figs. 10 and 11 increase to the same level (about ± 24.5 N·m), and the *d*-axis current shows similar changes as well. Overall, the dynamics of the new method is remarkable as well.

By comparing Figs. 11 and 12, slight reductions in the current and torque harmonics and ripples can be witnessed for the algorithm with delay compensation. Taking the condition that the machine runs at 100 rad/s as an example, the *q*-axis, *d*-axis, and torque ripples of the approach without delay compensation under the no-load conditions are about 11 A, 9 A, and 3.5 N·m, respectively, but they are 9.8 A, 8.3 A, and 3.2 N·m in Fig. 12, with a decrease of 10.9%, 7.8%, and 8.6%, respectively. Meanwhile, the results under load conditions see a similar trend to those under the no-load conditions. As far as the phase currents [see Figs. 11(b)–(d) and 12(b)–(d)] are concerned, the harmonics have been reduced visibly after the proposed delay compensation method is applied. These indicate that the proposed delay compensation method is effective for ripple reduction and performance improvement. In order to clearly observe the phase current ripples, Table IV lists the experimental THD analysis results under the rated load condition. First, compared with the values in Table II, the magnitude of THD is larger. The phenomenon arises mainly because the back EMF of the PMSM used for test is more like a square wave rather than a sine wave, and this should be also responsible for the low sinusoidal degree of phase current. It is expected that the proposed method is more effective for a PMSM with standard sine wave back EMF. Second, similar to the simulation results, the THD for the proposed FCS-MPC method with delay compensation is minimal among the three cases, indicating that the proposed method is effective.

Fig. 13 illustrates the experimental results (speed is 100 rad/s and load torque is 5 N·m) when the proposed multiobjective FCS-MPC is compensated by the traditional TSP-based (between 0 and 2 s) and the proposed dual-sampling-based (between 2 and 4 s) delay compensation strategies. Similar to the simulation results, the new method shows a slightly better performance. In detail, the THD of the phase current declines from 8.23% to 7.96%, and the *d*- and *q*-axis current ripples drop by nearly 3.5% and 4.9%, respectively. These indicate that the novel compensation strategy is totally suitable for the FCS-MPC applications.

V. Conclusion

This article proposes a multiobjective (speed and current) FCS-MPC strategy for the PMSMs, achieving simple single-closed-loop control topology. Besides, a novel computation delay compensation method is developed to lower the ripples and harmonics in the system. The main contributions of this article are as follows.

1) Compared with the traditional single-objective FCS-MPC algorithms, both speed and current are included into the cost function of the proposed FCS-MPC controller as the TCOs. By doing this, the speed controller is no longer needed. When designing the algorithms, an improved PMSM model, which contains not only differential but also integral equations is established, and an effective weighting factor handling strategy on the account of SVN and the balance of state sensitivity to voltage alteration is developed. Both the simulation and experimental results have comparatively verified the high steady-state and dynamic performance of the controller.
2) In order to suppress the current and torque ripples caused by the computation delay, a compensation scheme on the basis of dual sampling is proposed. The novel delay compensation scheme is composed of two sequential procedures: delay time estimation and compensation. The experimental results illustrate that the state ripples decrease by around 8% after compensation and the proposed delay compensation strategy has better performance in comparison with the traditional TSP technique.

Finally, it deserves to be mentioned that considering the speed regulation frequency equals the current regulation frequency for the proposed FCS-MPC method, in order to exert the optimal control capability in the ultralow speed range, the encoders with more lines are preferred when the current and speed updating frequency is high. Moreover, considering that the proposed FCS-MPC method is parameter dependent (e.g., the moment of inertia, flux, and inductance), it is necessary to incorporate the effective techniques that are able to enhance the robustness against parameter variations/mismatch into the control process in the future.

References

[1] Z. Q. Zhu and Y. Liu, "Analysis of air-gap field modulation and magnetic gearing effect in fractional-slot concentrated-winding permanent-magnet synchronous machines," *IEEE Trans. Ind. Electron.*, vol. 65, no. 5, pp. 3688–3698, May 2018.

[2] J. Lu, X. Zhang, Y. Hu, J. Liu, C. Gan, and Z. Wang, "Independent phase current reconstruction strategy for IPMSM sensorless control without using null switching states," *IEEE Trans. Ind. Electron.*, vol. 65, no. 6, pp. 4492–4502, Jun. 2018.

[3] C. Gong, Y. Hu, G. Chen, H. Wen, Z. Wang, and K. Ni, "A dc-bus capacitor discharge strategy for PMSM drive system with large inertia and small system safe current in EVs," *IEEE Trans. Ind. Inform.* vol. 15, no. 8, pp. 4709–4718, Aug. 2019.

[4] A. D. Alexandrou, N. K. Adamopoulos, and A. G. Kladas, "Development of a constant switching frequency deadbeat predictive control technique for field-oriented synchronous permanent-magnet motor drive," *IEEE Trans. Ind. Electron.*, vol. 63, no. 8, pp. 5167–5175, Aug. 2016.

[5] Y. Zhang and J. Zhu, "Direct torque control of permanent magnet synchronous motor with reduced torque ripple and commutation frequency," *IEEE Trans. Power Electron.*, vol. 26, no. 1, pp. 235–248, Jan. 2011.

[6] G. Wang, J. Qi, J. Xu, X. Zhang, and D. Xu, "Antirollback control for gearless elevator traction machines adopting offset-free model predictive control strategy," *IEEE Trans. Ind. Electron.*, vol. 62, no. 10, pp. 6194–6203, Oct. 2015.

[7] Y. Zhang, H. Yang, and B. Xia, "Model-predictive control of induction motor drives: Torque control versus flux control," *IEEE Trans. Ind. Appl.*, vol. 52, no. 5, pp. 4050–4060, Sep./Oct. 2016.

[8] M. Preindl and S. Bolognani, "Model predictive direct torque control with finite control set for PMSM drive systems—Part 1: Maximum torque per ampere operation," *IEEE Trans. Ind. Inform.*, vol. 9, no. 4, pp. 1912–1921, Nov. 2013.

[9] A. Mora, Á. Orellana, J. Juliet, and R. Cárdenas, "Model predictive torque control for torque ripple compensation in variable-speed PMSMs," *IEEE Trans. Ind. Electron.*, vol. 63, no. 7, pp. 4584–4592, Jul. 2016.

[10] S. Kwak, U.-C. Moon, and J.-C. Park, "Predictive-control-based direct power control with an adaptive parameter identification technique for improved AFE performance," *IEEE Trans. Power Electron.*, vol. 29, no. 11, pp. 6178–6187, Nov. 2014.

[11] E. Fuentes, C. A. Silva, and R. M. Kennel, "MPC implementation of a quasi-time-optimal speed control for a PMSM drive, with inner modulated-FS-MPC torque control," *IEEE Trans. Ind. Electron.*, vol. 63, no. 6, pp. 3897–3905, Jun. 2016.

[12] B. Stellato, T. Geyer, and P. J. Goulart, "High-speed finite control set model predictive control for power electronics," *IEEE Trans. Power Electron.*, vol. 32, no. 5, pp. 4007–4020, May 2017.

[13] A. Darba, F. De Belie, P. D'haese, and J. A. Melkebeek, "Improved dynamic behavior in BLDC drives using model predictive speed and current control," *IEEE Trans. Ind. Electron.*, vol. 63, no. 2, pp. 728–740, Feb. 2016.

[14] N. Jabbour and C. Mademlis, "Online parameters estimation and auto-tuning of a discrete-time model predictive speed controller for induction motor drives," *IEEE Trans. Power Electron.*, vol. 34, no. 2, pp. 1548–1559, Feb. 2019.

[15] M. Yang, X. Lang, J. Long, and D. Xu, "Flux immunity robust predictive current control with incremental model and extended state observer for PMSM drive," *IEEE Trans. Power Electron.*, vol. 32, no. 12, pp. 9267–9279, Dec. 2017.

[16] Y. A.-R. I. Mohamed and E. F. El-Saadany, "Robust high bandwidth discrete-time predictive current control with predictive internal model—A unified approach for voltage-source PWM converters," *IEEE Trans. Power Electron.*, vol. 23, no. 1, pp. 126–136, Jan. 2008.

[17] X. Zhang, L. Zhang, and Y. Zhang, "Model predictive current control for PMSM drives with parameter robustness improvement," *IEEE Trans. Power Electron.*, vol. 34, no. 2, pp. 1645–1657, Feb. 2019.

[18] W. Wang, Y. Fan, S. Chen, and Q. Zhang, "Finite control set model predictive current control of a five-phase PMSM with virtual voltage vectors and adaptive control set," *CES Trans. Elect. Mach. Syst.*, vol. 2, no. 1, pp. 136–141, Mar. 2018.

[19] J. Liu, C. Gong, Z. Han, and H. Yu, "IPMSM model predictive control in flux-weakening operation using an improved algorithm," *IEEE Trans. Ind. Electron.*, vol. 65, no. 12, pp. 9378–9387, Dec. 2018.

[20] F. Wang, X. Mei, J. Rodriguez, and R. Kennel, "Model predictive control for electrical drive systems—An overview," *CES Trans. Elect. Mach. Syst.*, vol. 1, no. 3, pp. 219–230, Sep. 2017.

[21] W. Xie *et al.*, "Finite-control-set model predictive torque control with a deadbeat solution for PMSM drives," *IEEE Trans. Ind. Electron.*, vol. 62, no. 9, pp. 5402–5410, Sep. 2015.

[22] F. Ban, G. Lian, J. Zhang, B. Chen, and G. Gu, "Study on a novel predictive torque control strategy based on the finite control set for PMSM," *IEEE Trans. Appl. Supercond.*, vol. 29, no. 2, pp. 1–6, Mar. 2019.

[23] Y. Yan, S. Wang, C. Xia, H. Wang, and T. Shi, "Hybrid control set-model predictive control for field-oriented control of VSI-PMSM," *IEEE Trans. Energy Convers.*, vol. 31, no. 4, pp. 1622–1633, Dec. 2016.

[24] W. Tu, G. Luo, R. Zhang, Z. Chen, and R. Kennel, "Finite-control-set model predictive current control for PMSM using grey prediction," in *Proc. IEEE Energy Convers. Congr. Expo.*, Milwaukee, WI, USA, 2016, pp. 1–7.

[25] M. Preindl and S. Bolognani, "Model predictive direct speed control with finite control set of PMSM drive systems," *IEEE Trans. Power Electron.*, vol. 28, no. 2, pp. 1007–1015, Feb. 2013.

[26] M. Preindl and S. Bolognani, "Model predictive direct speed control with finite control set of PMSM-VSI drive systems," in *Proc. Workshop Predictive Control Elect. Drives Power Electron.*, Munich, Germany, 2011, pp. 17–23.

[27] C. Gong, Y. Hu, K. Ni, J. Liu, and J. Gao, "SM load torque observer-based FCS-MPDSC with single prediction horizon for high dynamics of surface-mounted PMSM," *IEEE Trans. Power Electron.*, vol. 35, no. 1, pp. 20–24, Jan. 2020.
[28] A. Formentini, A. Trentin, M. Marchesoni, P. Zanchetta, and P. Wheeler, "Speed finite control set model predictive control of a PMSM fed by matrix converter," *IEEE Trans. Ind. Electron.*, vol. 62, no. 11, pp. 6786–6796, Nov. 2015.
[29] E. J. Fuentes, C. A. Silva, and J. I. Yuz, "Predictive speed control of a two-mass system driven by a permanent magnet synchronous motor," *IEEE Trans. Ind. Electron.*, vol. 59, no. 7, pp. 2840–2848, Jul. 2012.
[30] F. Mwasilu, H. T. Nguyen, H. H. Choi, and J.-W. Jung, "Finite set model predictive control of interior PM synchronous motor drives with an external disturbance rejection technique," *IEEE/ASME Trans. Mechatronics*, vol. 22, no. 2, pp. 762–773, Apr. 2017.
[31] P. Cortes *et al.*, "Guidelines for weighting factors design in model predictive control of power converters and drives," in *Proc. IEEE Int. Conf. Ind. Technol.*, Gippsland, VIC, Australia, 2009, pp. 1–7.
[32] Y. Wang *et al.*, "Deadbeat model-predictive torque control with discrete space-vector modulation for PMSM drives," *IEEE Trans. Ind. Electron.*, vol. 64, no. 5, pp. 3537–3547, May 2017.
[33] X. Zhang, B. Hou, and Y. Mei, "Deadbeat predictive current control of permanent-magnet synchronous motors with stator current and disturbance observer," *IEEE Trans. Power Electron.*, vol. 32, no. 5, pp. 3818–3834, May 2017.
[34] Y. Yang, H. Wen, and D. Li, "A fast and fixed switching frequency model predictive control with delay compensation for three-phase inverters," *IEEE Access*, vol. 5, pp. 17904–17913, 2017.
[35] X. Xiao, Y. Zhang, J. Wang, and H. Du, "An improved model predictive control scheme for the PWM rectifier-inverter system based on power-balancing mechanism," *IEEE Trans. Ind. Electron.*, vol. 63, no. 8, pp. 5197–5208, Aug. 2016.
[36] J. Guzinski, H. Abu-Rub, M. Diguet, Z. Krzeminski, and A. Lewicki, "Speed and load torque observer application in high-speed train electric drive," *IEEE Trans. Ind. Electron.*, vol. 57, no. 2, pp. 565–574, Feb. 2010.
[37] A. Waheed and L. Cai, "Alternative design for optical incremental encoder measurement systems," in *Proc. IEEE Int. Conf. Ind. Technol.*, Taipei, Taiwan, 2016, pp. 634–639.

Yaofei Han (Member, IEEE) was born in Henan, China. He received the M.S. and the Ph.D. degrees in power electronics and drives from the China University of Mining and Technology, Xuzhou, China, in 2005 and 2010, respectively.

Since 2010, he has been with the Henan University of Urban Construction, where he has been an Associate Professor since 2012. From 2017 to 2019, he was with the School of Electrical and Computer Engineering, Virginia Polytechnic Institute and State University, as a Visiting Scholar. He is currently with the School of Electronic Information and Electrical Engineering, Shanghai Jiao Tong University, Shanghai, China. His research interests include multilevel power converters for power conversion and motor control and the high-efficiency converter for renewable power conversion system.

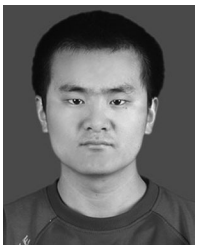

Chao Gong (Student Member, IEEE) was born in Shandong province in China, on February 22, 1991. He received the B.Eng. and M.Eng. degrees in electrical engineering from the Northwestern Polytechnical University, Xi'an, China, in 2014 and 2016, respectively. He is currently working toward the Ph.D. degree with the major of electrical engineering with the Department of Electrical Engineering and Electronics, University of Liverpool, Liverpool, U.K.

His research interests include electrical machines design and drives, power electronics, and motion control.

Liming Yan (Student Member, IEEE) was born in Shaanxi, China, in 1988. He received the B.S. degree in software engineering from Chang'an University, Xi'an, China, in 2011, the M.S. degree in electric machine and electric apparatus from the Shenyang University of Technology, Shenyang, China, in 2014, and the Ph.D. degree in electrical engineering from the Northwestern Polytechnical University, Xi'an, China, in 2019.

He is currently working with Chang'an University, Xi'an, China. His research interests include the model predictive control of power electronics and electrical drives.

Huiqing Wen (Senior Member, IEEE) received the B.S. and M.S. degrees in electrical engineering from Zhejiang University, Hangzhou, China, in 2002 and 2006, respectively, and the Ph.D. degree in electrical engineering from the Chinese Academy of Sciences, Beijing, China, in 2009.

From 2009 to 2010, he was an Electrical Engineer with the GE (China) Research and Development Center Company, Ltd., Shanghai, China. From 2010 to 2011, he was an Engineer with the China Coal Research Institute, Beijing, China. From 2011 to 2012, he was a Postdoctoral Fellow with the Masdar Institute of Science and Technology, Abu Dhabi, United Arab Emirates. In 2013, he joined the Electrical and Electronic Engineering Department of Xi'an Jiaotong-Liverpool University (XJTLU), Suzhou, China. He is currently a Senior Associate Professor with the XJTLU. He has authored or coauthored more than 100 peer-reviewed technical papers in leading journals/conferences and holds over 20 issued/pending patents. His research interests include renewable energy, electric vehicle, power electronics, microgrid, and power semiconductor devices.

Dr. Wen is the Associate Editor for the *IEEE Access*, the *International Journal of Photoenergy*, and the *Journal of Power Electronics*.

Yangang Wang (Senior Member, IEEE) received the Ph.D. degree in microelectronics and solid-state electronics from Peking University, Beijing, China, in 2007.

In 2012, he joined as a Principal Engineer with the R&D Centre of CRRC Dynex Semiconductor, Ltd., Lincoln, U.K., where he is currently in the leading role of the department responsible for the development of advanced Si and wide-bandgap power semiconductor products. He has more than 20-year research and development work experience in microelectronics and power electronics. His current research and development activities include design/simulation, packaging, test/characterization, failure analysis, reliability and lifetime prediction etc. for power Si and WBG semiconductor devices.

Dr. Wang is a member of IET and a Chartered Engineer of the U.K.

Ke Shen (Member, IEEE) received the B.S., M.S., and Ph.D. degrees in electrical engineering from the Harbin Institute of Technology, Harbin, China, in 2007, 2009, and 2014, respectively.

From 2011 to 2012, he was a Visiting Ph.D. Student with the Center for Ultra-Wide-Area Resilient Electric Energy Transmission Networks, University of Tennessee, Knoxville. Since 2014, he has been with the School of Automation, Northwestern Polytechnical University, Xi'an, China, where he is currently an Assistant Professor. His current research interests include power electronics, multilevel converters, and energy conversion.